An article presented by the group of Dr. Majd Al-Naji from the Max Planck Institute of Colloids and Interfaces (Germany).

Controlled lignosulfonate depolymerization *via* solvothermal fragmentation coupled with catalytic hydrogenolysis/hydrogenation in a continuous flow reactor

Sodium lignosulfonate as a side stream product from the pulp industry was valorized in a continuous flow system using solvothermal fragmentation independently, as well as combined with a catalytic hydrogenolysis/hydrogenation step. Using this simple and tunable process, sodium lignosulfonate was simultaneously deconstructed towards high monomer yields or low molecular weight oligomers. Thus, this approach can potentially be applied for the production of both fine chemicals and smart materials.

As featured in:

See Majd Al-Naji *et al.*, *Green Chem.*, 2021, **23**, 9894.

ROYAL SOCIETY OF CHEMISTRY

rsc.li/greenchem

PAPER

Controlled lignosulfonate depolymerization *via* solvothermal fragmentation coupled with catalytic hydrogenolysis/hydrogenation in a continuous flow reactor†

Francesco Brandi, [iD] Markus Antonietti [iD] and Majd Al-Naji [iD] *

Sodium lignosulfonate (LS) was valorized to low molecular weight (M_w) fractions by combining solvothermal (SF) and catalytic hydrogenolysis/hydrogenation fragmentation (SHF) in a continuous flow system. This was achieved in either alcohol/H_2O (EtOH/H_2O or MeOH/H_2O) or H_2O as a solvent and Ni on nitrogen-doped carbon as a catalyst. The tunability according to the temperature of both SF and catalytic SHF of LS has been separately investigated at 150 °C, 200 °C, and 250 °C. In SF, the minimal M_w was 2994 g mol^{-1} at 250 °C with a dispersity (*Đ*) of 5.3 using MeOH/H_2O. In catalytic SHF using MeOH/H_2O, extremely low M_w was found (433 mg g$_{LS}^{-1}$) with a *Đ* of 1.2 combined with 34 mg g$_{LS}^{-1}$. The monomer yield was improved to 42 mg g$_{LS}^{-1}$ using dual catalytic beds. These results provide direct evidence that lignin is an unstable polymer at elevated temperatures and could be efficiently deconstructed under hydrothermal conditions with and without a catalyst.

Introduction

In the last few centuries, extensive exploitation of fossil resources has led to the current global environmental challenges that we are facing.[1–4] A transition toward more sustainable and renewable resources and production processes for energy and commodities is in great demand.[5–11] Among the renewable resources, lignocellulosic biomass (LCB) is one of the most promising feedstock since it is abundant, cheap, and intrinsically sustainable as it is produced *via* photosynthesis by plants.[12–14] LCB is a complex solid composite, made of three biopolymers: cellulose, hemicellulose, and lignin.[13,15,16] Currently, LCB is industrially processed on the Gt scale per year, and about 4 Gt of wood products are made every year, with about 1 Gt ending in pulp and paper factories.[16,17] Within the scope of the current article, it is important to note that only the sugar fractions are valorized, *e.g.* as pulp. The remaining lignin (which can be isolated nowadays as a by-product) is used in some product streams with lower capacity, but is mostly used for energy and heat generation *via* combustion.[18–22] Moving toward a more sustainable and mature biorefinery is a broadly proclaimed target, and is based on efficient valorization of all LCB components, including

lignin.[23–28] In 2007, the U.S. Department of Energy (DoE) report posed a milestone for lignin valorization and defined the bio-economy of lignin.[29] Accordingly, in the report three major valorization scenarios for lignin were defined with respect to their usage in the future: 1st combustion for energy purposes (short term), 2nd application of lignin as a macromolecule (middle term), and 3rd application of lignin as a source of aromatic monomers and oligomers (long term).

Lignin is a complex three-dimensional network of cross-linked phenylpropanoid units connected through different types of ether bonds, *i.e.*, β–O–4, 4–O–5, γ–O–α, and carbon–carbon bonds, *e.g.*, 5–5 and β–β linkages, *viz.* Fig. 1.[15,30–34] Some of the big challenges in lignin valorization are its heterogeneity, recalcitrance against treatments, and the sensitivity of lignin fragments for follow-up condensation reactions.[12,30] Currently, four main technologies are used to separate lignin from the other biomass components, *i.e.*, kraft, soda, organosolv and sulfite processes.[21,30,35,36] These processes rely on lignin separation from the LCB matrix *via* solubilization by applying harsh conditions with pH = 1–5 for sulfite and organosolv or pH = 11–13 for soda and kraft, as well as high temperatures (140–220 °C).[21,37] The resulting lignin is named technical lignin and is indeed different from the primary plant product.[21,37] In the DoE Report, the technical lignin is proposed as the most probable future source of lignin since it is abundant and already available from industrial processes, such as the pulping process.[29] Nowadays, the 1st scenario is still the major application of technical lignin and every year,

Max Planck Institute of Colloids and Interfaces, Colloid Chemistry Department, Am Mühlenberg 1, 14476 Potsdam, Germany. E-mail: majd.al-naji@mpikg.mpg.de

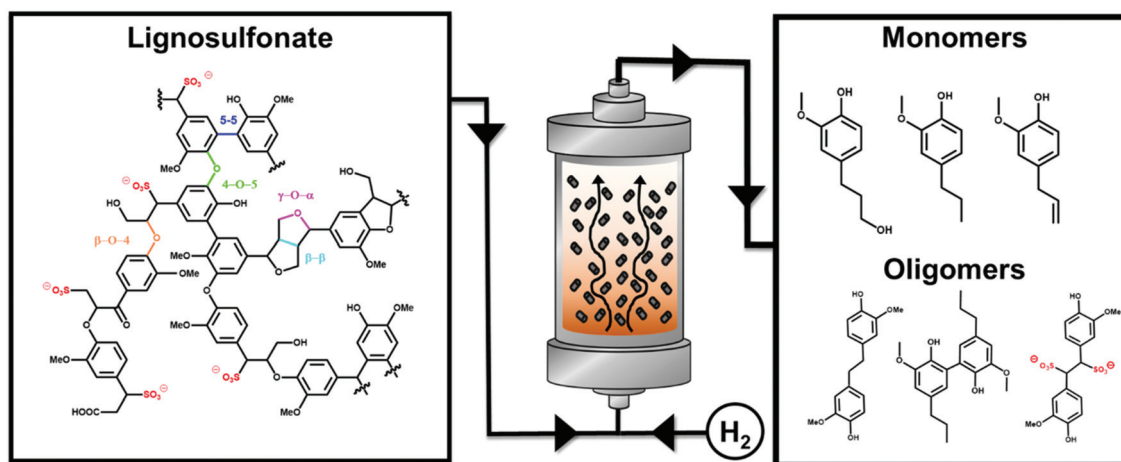†Electronic supplementary information (ESI) available. See DOI: 10.1039/d1gc01714d

Fig. 1 Route of controlled sodium lignosulfonate (LS) valorization using a continuous flow system.

from the principal 250 Mt, about ~70 Mt of technical lignin is separated, of which an estimated 95% is burned to produce energy.[38,39] Of that amount, approximately 2 Mt per y are produced only by the sulfite process.[21,38]

In the sulfite pulping, debarked wood chips are treated with sulfite and bisulfite salt solution (Na is the major counter-ion to bisulfite) in acidic aqueous media (pH 1–5) at temperatures ranging from 125 to 190 °C.[21,40] In this process, the ether bonds in lignin are partially hydrolyzed followed by the sulfitization step (introducing –SO_3^- functionalities), or oxidative coupling to form parasitic C–C bonds.[21,29] Consequently, the resulting technical lignin is named sodium lignosulfonate (LS). It possesses a wide range of molecular weight (M_w) from 1000 to 100 000 g mol^{-1}, the obtained M_w values depend on process severity.[21] LS contains a large amount of sulfur (3 to 8 wt%) and a reduced number of C–O bonds (Fig. 1) compared to the native lignin in wood.[30] Uniquely, LS is highly water-soluble due to the presence of SO_3^- groups. Sulfonate endows LS with surfactant properties and it is used in current materials applications as a macro-molecule (2nd scenario), e.g., as superplasticizer in cements and clays,[41] and as dispersing agents for polymeric foams,[42,43] dyes[44] and colloidal dispersions.[45,46] Additionally, LS has been used to create completely new lignin-based materials, e.g., bio-composites for fire-retardant thermal insulators,[47,48] or S-doped carbonaceous materials for high-performance electro-chemical devices such as batteries and supercapacitors.[47,49,50] All the abovementioned applications have been reported to depend strongly on the molecular weight distribution (M_w) of the obtained LS.[20,48,51]

As LS has a high phenolic content, it also shows great potential for the production of bio-based aromatics via oxi-dative or reductive catalytic fractionation (O or RCF) and is considered the 3rd scenario.[45,52–56] In the last decade, RCF, pioneered by the Sels group, has been reported as one of the methods with the highest potential for lignin valorization towards phenolic single units, mostly starting directly from

wood.[12,23,28,57–62] Based on this process, an approach for the valorisation of lignin toward both phenolic monomers and phenolic oligomers has been proposed to scale up such a process to industry.[23,63] The simultaneous valorization of monomers and dimers in such an approach has the potential to provide a further step toward the complete usage of lignin in the biorefinery.

Despite the potential of RCF, few studies have been reported using LS solutions. To this end, Shu et al.[53] reported LS hydrogenolysis using a Pt on a carbon catalyst and CrCl$_3$ homogeneous co-catalyst at 280 °C, 3 MPa of H$_2$, in batch systems. Additionally, the effect of a Ni and Mo bimetallic catalyst on Al$_2$O$_3$ was studied in ethylene glycol and super-critical ethanol at 310 °C and 26 bar of H$_2$ in batch systems.[64,65] This approach led to LS fragmentation mostly towards dimers and oligomers resulting in an optimized 88 wt% oil yield, while the minor fraction of monomers was only qualitatively studied.[64,65] All these studies were per-formed in batch systems, which present disadvantages when compared to continuous flow systems, e.g., complex product–catalyst separation, time and energy-consumption in discon-tinuous steps and cost efficiency.[10,12,59,66,67] Horáček et al.[52] reported only the LS fragmentation in a continuous flow system at a high reaction temperature (320 °C) over a bi-metallic Ni and Mo catalyst supported on Al$_2$O$_3$. In this study and due to over hydrogenation, guaiacol was found as the major product of LS catalytic fragmentation (yield higher than 1.8 wt%).

Herein, we investigate the LS depolymerization in a con-tinuous flow system under mild reaction conditions using the water/alcohol solvent system. In addition, the effect of catalyst-free solvothermal fragmentation (SF) of LS to low M_w fractions and phenolic monomers was explored. Furthermore, the latter step was coupled to hydrogenolysis/hydrogenation fragmenta-tion (SHF) in a continuous flow system using the water/alcohol solvent and 35 wt% Ni supported on NDC as a catalyst.[68,69] Finally, the advantage of operating the catalytic depolymeriza-

tion of LS in a continuous flow system is highlighted with respect to the batch system.

Experimental section

Materials

All the materials, including sodium lignosulfonate (LS), were utilized as received without further purification. The complete list of chemicals used, suppliers, and purities can be found in section S1 of the ESI.†

Catalyst synthesis and characterization

A pelletized catalyst of 35 wt% Ni deposited on nitrogen-doped carbon (35Ni/NDC) has been synthesized and characterized following the "kitchen lab" approach, as previously reported by our group, *cf.* sections S2 and S3 in the ESI.†[68] The catalyst was characterized *via* combustion elemental analysis (EA), inductively coupled plasma (ICP) optical emission spectroscopy elemental analysis, N2 physisorption, powder X-ray diffraction (XRD), thermogravimetric analysis (TGA), high-resolution scanning transmission electron microscopy (HR-STEM), and energy-dispersive X-ray spectrometry (EDS) and CO-chemisorption. All procedures of catalyst characterization are described in detail in section S3 in the ESI.†

Continuous flow setup

Liquid-phase LS depolymerization using water/alcohol solvent mixtures was conducted in a continuous flow fixed bed reactor, similar to our previously described system (Fig. S2 in the ESI†).[68–70]

This system consists of: (A) an HPLC pump equipped with a pressure sensor (Knauer Azura P 4.1S Series), (B) a mass-flow controller to supply a specific H_2 flow (Model SLA58050 from Brooks), (C) a T-piece for the gas–liquid mixer (Swagelok SS-400-30) to mix the supplied H_2 with the reaction solution before reaching the pre-heating unit and the catalyst bed, (D) a two-side open heating unit equipped with a heat controller (Model # 4848 from Parr Instrument Company), and (E) a sampling unit equipped with proportional relief valves also used as a pressure regulator (Swagelok SS-RL4M8F8-EP), *cf.* Fig. S2 in the ESI.† To ensure efficient heating, a cylindrical aluminium adapter with three boreholes was matched inside the heating unit. One bore is used for the preheating unit for the reactant before it comes in contact with the catalyst, another hole for the thermocouple (Model # A472E5 Parr Instrument Company) and the third one for the tubular reactor (Fig. S3 in the ESI†). The reactions were performed in a stainless steel tubular reactor (inner diameter = 21 mm, outer diameter = 25 mm, length = 280 mm), *viz.* Fig. S4 in the ESI.† Finally, an experiment using two consecutive fixed bed reactors filled with 10 g each of 35Ni/NDC was conducted. To perform these experiments two fixed bed reactors (D1–D2) were coupled in a setup similar to the one described above (Fig. S5 in the ESI†).

Catalytic experiments

Prior to each experiment, the LS solution (c_{LS} = 1.0 wt% or 2.5 wt%) was filtered through filter paper (Whatman™ grade 40, 8 μm) to remove any solid residues that could cause clogging of the continuous flow system. In a typical experiment, the solution of LS was fed by the HPLC pump at 1.0 cm^3 min^{-1}, then mixed with H_2 (20 cm^3 min^{-1}) and passed through the preheating unit and the tubular reactor. The temperature and pressure were kept constant (25 °C and atmospheric pressure) for 30 minutes at this steady state. Afterwards, the system was pressurized to 7.0 MPa to ensure the presence of the water/alcohol solvent system in the liquid state. Later, the system was heated to the desired reaction temperature (150 °C, 200 °C and 250 °C). In each catalytic experiment, 10 g of catalyst mass was used. Samples (30 cm^3) were collected once the steady-state was reached (*ca.* 60 min). For the time on stream (TOS) experiment, samples were collected after 1 h, 3 h, 6 h, and 9 h of TOS. In the case of the two coupled reactors, a second, similarly filled reactor was mounted after the first reactor, and the same conditions were used as in the single reactor experiments. Samples were collected once both systems reached the steady-state (*ca.* 120 min).

The collected samples were injected into a size exclusion chromatography (SEC) system without further processing, while the product analysis procedure was established to separate the residual LS from the reaction mixture, and therefore analyze the separated mixtures by GC-MS, GC-FID, 2D HSQC NMR, FTIR, elemental analysis and EDS. The established product analysis procedure is described in detail in the ESI in section S5.†

The batch experiment was conducted in a stainless steel autoclave equipped with PTFE liners and a magnetic stirrer from Berghof (Model: BR-100). The catalytic experiments were performed at 250 °C using 30 cm^3 of LS solution in a MeOH/H_2O solvent mixture (c_{LS} = 2.5 wt%) with 1.0 g of 35Ni/NDC and 7.0 MPa of external H_2 pressure for 1 and 3 h. Prior to heating to 250 °C, air was purged out using 1.0 MPa of N_2 three times. The analysis of the reaction products followed the same protocol that was established for the continuous flow experiments.

Results and discussion

Composition analysis of sodium lignosulfonate

Initially, the chemical composition of the utilized commercially available sodium lignosulfonate (LS) was investigated *via* elemental analysis, (Table 1). The LS was found to contain 7.0 wt% of sulfur (Table 1). This S content is comparable to the reported industrial sulfite process by Borregaard.[21,43] This indicates a high sulfonation degree and consequentially a high content of counter ions. In this context, Na was found to be the major sulfonate counter ion with 10 wt%, combined with the presence of Ca and Mg traces (Table 1). The presence of these Ca and Mg ions points to the usage of mixed sulfite salts

Table 1 Chemical composition, and textural and size properties of LS

Entry	C^a/wt%	S^b/wt%	O^a/wt%	H^a/wt%	Na^c/wt%	Ca^c/wt%	Mg^c/wt%	$M_w{}^d$/g mol^{-1}	$Đ^d$
LS	40	7.0	36	4.0	10	1.0	0.10	12 390	9.1
SHF-LS^e	39	5.0	34	4.6	9.4	0.8	0.10	433	1.2

^{a} Measured *via* EA analysis. ^{b} Measured by EDS. ^{c} Measured *via* ICP-OES. ^{d} Calculated by SEC. ^{e} Referred to the SHF-MeOH/H$_2$O experiment.
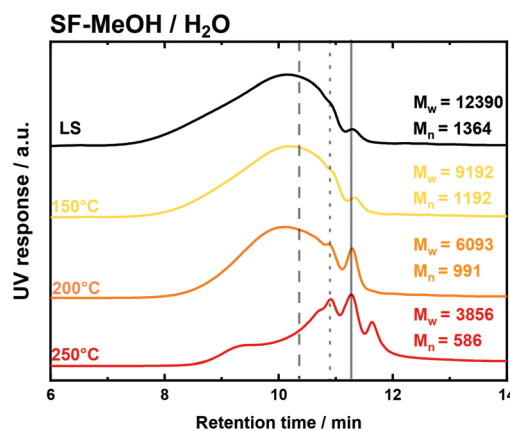
containing Na, Ca and Mg in the industrial isolation process.[21] Moreover, TGA analysis for LS showed a relatively high residual mass at 700 °C of 56 wt%, confirming the high sulfonation degree, *cf.* Fig. S7 in the ESI.† Finally, the moisture content was found to be 4.5 wt%, as determined by TGA analysis (see Table 1 and Fig. S7 in the ESI†).

The SEC analysis of an aqueous LS solution (1 wt%) showed a weight average molecular weight (M_w) of 12 390 g mol^{-1} with a dispersity ($Đ$) of 9.1, *viz.* Fig. S8 in the ESI.† This high $Đ$ value indicates that LS presents a polydisperse distribution of the molecular weight. The 2D HSQC NMR spectra of the LS showed the absence of syringyl units (S), and only guaiacyl units (G) have been found in the typical aromatic region (δ_C/δ_H 100–150/6.2–7.5), *viz.* Fig. S9 in the ESI.†[71,72] This indicates that the utilized LS in this work has been produced from softwood, in which the S/G molar ratio is zero. Generally, lignin rich in G units is favorable for certain applications such as additives for polymers and resins. This is due to the reactive *ortho*-position of the phenolic rings, which promotes radical-initiated crosslinking.[73] 2D HSQC NMR of LS showed the presence of sulfo-groups in the α position (α-S$_{α,β,γ}$) at δ_C/δ_H of 66–68/4.5–4.7, 79–82/4.7–5.1 and 60–62/3.9–4.0, respectively. These are typical for LS, *viz.* Fig. S9 in the ESI.†[71,72] Moreover as expected, FTIR analysis showed the typical O–H stretching bond at around 3400 cm^{-1}, the asymmetric and symmetric O=S=O stretching at 1150–1200 cm^{-1} and 1036 cm^{-1} and the typical signals of the aromatic ring vibration at around 1400 cm^{-1} respectively, *viz.* Fig. S10 and Table S1 in the ESI.†[74]

Solvothermal fragmentation (SF) of sodium lignosulfonate

The usage of short chain bio-derivable alcohol such as ethanol (EtOH) and methanol (MeOH), as well as their mixture with water, has been reported as efficient solvent mixtures for both lignin extraction and fractionation.[57,75–78] Due to the low solubility of LS in organic solvents, an aqueous solvent mixture, *i.e.*, MeOH/H$_2$O and EtOH/H$_2$O, is necessary.[39] Therefore, the efficiency of water/alcohol mixtures (MeOH/H$_2$O and EtOH/H$_2$O with 1 : 1 weight ratio) and of pure H$_2$O as a solvent was studied for the catalyst-free solvothermal fragmentation (SF) of LS.

The solvothermal fragmentation reactions (SF) were performed at 150 °C, 200 °C, and 250 °C in the absence of the catalyst. In all cases, *i.e.*, using MeOH/H$_2$O and EtOH/H$_2$O mixtures and H$_2$O as the solvent, the SEC elugrams exhibited the successive disappearance of the peak at low retention times (<10 min), corresponding to the high molecular weight fraction, *cf.* Fig. 2 and Fig. S11 in the ESI.† For the MeOH/H$_2$O solvent mixture, the derived mass average molecular weight
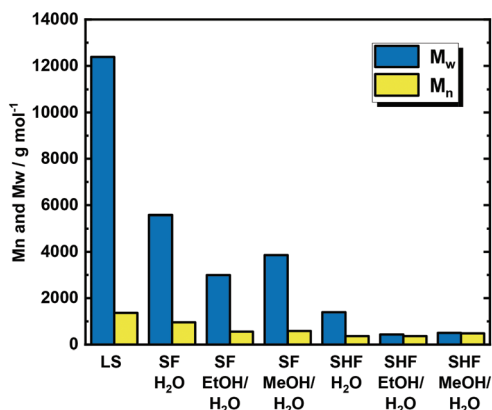

Fig. 2 SEC chromatograms of the solvothermal fragmentation (SF) of LS in MeOH/H$_2$O. Reaction conditions: c_{LS} = 1.0 wt%, T = 150 °C, 200 °C and 250° C, p = 7.0 MPa, Q_{educt} = 1.0 cm^3 min^{-1}, Q_{H_2} = 20 cm^3 min^{-1} and $t_{residence}$ = 50 min. The straight line indicates the eluent buffer reference peak (NaHPO$_3$), dotted and dashed lines show the analytical standard peaks, *i.e.*, sodium poly-(styrene sulfonate), with a M_w of 246 g mol^{-1} (RT = 10.9 min) and M_w of 891 g mol^{-1} (RT = 10.4 min), respectively.

(M_w) was decreased from 12 390 g mol^{-1} for untreated LS to 9132 g mol^{-1}, 6093 g mol^{-1} and 3856 g mol^{-1} following the increase of reaction temperature to 150 °C, 200 °C and 250 °C, respectively (Fig. 2, Table S2 – entries 2 to 4 and Fig. S12 in the ESI†). Similarly, the EtOH/H$_2$O solvent mixture showed a decrease of M_w with the increase of reaction temperatures, *i.e.*, from 150 °C to 200 °C and to 250 °C, giving the lowest M_w value of 3000 g mol^{-1} at 250 °C, *viz.* Fig. 3, Table S2 – entries 5 to 7 and Fig. S12 in the ESI.† Also using pure H$_2$O as a solvent, the M_w was found to be following the same behaviour, *i.e.* decreasing with the temperature increase, with the lowest M_w of 5578 g mol^{-1} at 250 °C (Fig. 3, Table S2 – entries 8 to 10 and Fig. S12 in the ESI†). Analogously to M_w, the number averaged molecular weight distribution (M_n) decreased with the increase of the reaction temperatures, giving the minimum at 250 °C, *i.e.*, M_n = 586 g mol^{-1}, 556 g mol^{-1} and 957 g mol^{-1} for MeOH/H$_2$O, EtOH/H$_2$O and H$_2$O respectively, *cf.* Fig. S12 and Table S2 – entries 4, 7, and 10 in the ESI.†

The significant decrease in the molecular weight in all cases indicates that the cleavage of the weaker linkages of LS (mostly phenyl ether bonds) has already occurred at the lower reaction temperatures, *i.e.*, 150 °C and 200 °C. Rather expectedly, this fragmentation is becoming most effective at the highest applied temperature, *i.e.*, 250 °C. However, the molecular weight dispersity ($Đ$) was found to be higher than 5.0 at

Paper

Fig. 3 Mass average molecular weight (M_w) and number average molecular weight (M_n) calculated from SEC curves for the solvothermal fragmentation (SF) of LS and solvothermal combined with catalytic hydrogenolysis/hydrogenation (SHF) using MeOH/H₂O, EtOH/H₂O, and H₂O solvent systems. Reaction conditions of SF: c_{LS} = 1.0 wt%, T = 250° C, p = 7.0 MPa, Q_{educt} = 1.0 cm³ min⁻¹, Q_{H_2} = 20 cm³ min⁻¹ and $t_{residence}$ = 50 min. Reaction conditions of SHF: c_{LS} = 1.0 wt%, T = 250° C, p = 7.0 MPa, Q_{educt} = 1.0 cm³ min⁻¹, Q_{H_2} = 20 cm³ min⁻¹, $m_{35Ni/NDC}$ = 10 g, $t_{residence}$ = 50 min, and weight hour space velocity (WHSV) = 0.17 g_{LS} h⁻¹ g_{Ni}⁻¹.

all of the investigated temperatures using all solvent systems (Table S2 – entries 2 to 10 – in the ESI†). This indicates that fragmentation occurred only partially, resulting in a heterogeneous mixture with different sizes of oligomers, mostly tri-, tetra- and pentamers. An additional explanation for such a heterogeneous molar mass distribution could be attributed to *in situ* re-polymerization (side reactions) of the cleaved intermediates or the occurrence of radical polymerization.[79] Nonetheless, the water/alcohol mixtures exhibited lower molar mass distributions over all the investigated temperatures. This result is attributed to the better stabilization of the intermediates against re-condensation by water/alcohols mixtures. Based on this, MeOH/H₂O and EtOH/H₂O samples were selected to

qualitatively analyse the monomers using GC-MS, *viz*. Fig. S13 in the ESI.† From this chromatogram, a wide range of monomers (16 compounds) has been identified and reported in Table S3 in the ESI.† Moreover, the GC-MS chromatogram exhibited peaks in the high retention time region (>20 min), which can be attributed to dimers. However, these dimers were not identified and recognized by the compound database of the GC device. Among the identified compounds, 4-propyl guaiacol (G1), 4-ethyl guaiacol (G2), homovanillyl alcohol (G3), dihydroconiferyl alcohol (G4), guaiacol (G5) creosol (G6), eugenol (G7) and isoeugenol (G8) were quantified using GC-FID, and cumulative monomer yields of 8.7 mg g_{LS}⁻¹ and 2.9 mg g_{LS}⁻¹ were calculated for MeOH/H₂O and EtOH/H₂O, respectively (Table 2 and Fig. S14 in the ESI†). These higher cumulative monomer yields are attributed to better monomer stabilization by the MeOH/H₂O solvent mixtures. It is noteworthy to be mentioned here that SF in continuous flow systems produced partially depolymerized LS. In this simple approach, the molecular weight distribution has been found to depend directly on the reaction temperature. This finding can be attributed to the thermal elimination of single phenol units from LS. This is a typical behaviour of a thermodynamically unstable polymer that undergoes reversible addition–fragmentation reactions. Moreover, the derived dispersity (Đ = 6.5 at 250 °C using MeOH/H₂O) indicates that this equilibrium is perturbed by side reactions such as condensation of the cleaved fragments. This phenomenon provides clear evidence of the presence of a ceiling temperature, above which the polymer is spontaneously depolymerized into smaller units. Interestingly, the presence of a ceiling temperature is a general phenomenon in polymer science but was mostly not reported in the community of lignin biorefinery.[80]

Solvothermally assisted catalytic hydrogenolysis/hydrogenation fragmentation (SHF) of sodium lignosulfonate

Primarily, the utilized 35Ni/NDC in pellet form was synthesized using our "kitchen lab" approach that was previously

Table 2 Yield of the quantified monomers in the SF and SHF experiments. Monomers: 4-propyl guaiacol (G1), 4-ethyl guaiacol (G2), homovanillyl alcohol (G3), dihydroconiferyl alcohol (G4), guaiacol (G5), creosol (G6), eugenol (G7), isoeugenol (G8), and 4-propyl phenol (H1). The compound structure and the reaction conditions are reported in the main body of the manuscript

Sample	c_{LS}/ wt%	T/ °C	G1/mg g_{LS}⁻¹	G2/mg g_{LS}⁻¹	G3/mg g_{LS}⁻¹	G4/mg g_{LS}⁻¹	G5/mg g_{LS}⁻¹	G6/mg g_{LS}⁻¹	G7/mg g_{LS}⁻¹	G8/mg g_{LS}⁻¹	H1/mg g_{LS}⁻¹	Y_{CM}/mg g_{LS}⁻¹	STY$_{CM}$/mg h⁻¹ g_{Ni}⁻¹
SF-MeOH/ H₂O	1	250	1.2	0.48	1.5	0.94	0.80	0.04	3.4	0.35	n.a.	8.7	n.a.
SF-EtOH/H₂O	1	250	0.89	0.01	n.a.	0.94	0.93	0.05	n.a.	0.10.	n.a.	2.9	n.a.
SHF-MeOH/ H₂O	1	150	6.7	0.22	n.a.	0.72	0.80	0.46	n.a.	n.a.	0.19	9.1	1.6
	1	200	6.6	0.35	2.9	5.1	0.89	0.04	n.a.	n.a.	0.37	16	2.7
	1	250	16	2.7	3.1	8.2	2.2	0.22	n.a.	n.a.	0.83	34	5.8
SHF-EtOH/ H₂O	1	150	n.a.	n.a.	n.a.	0.72	1.0	n.a.	n.a.	n.a.	0.04	1.7	0.29
	1	200	2.4	0.12	0.6	2.6	0.61	0.01	n.a.	n.a.	0.04	6.3	1.1
	1	250	17	0.72	2.4	9.7	0.78	0.10	n.a.	n.a.	0.53	31	5.3
Flow 2.5 wt%	2.5	250	16	4.9	0.71	5.6	3.7	1.6	n.a.	n.a.	0.1	33	14
Dual column	2.5	250	20	5.7	0.94	9.6	3.4	1.6	n.a.	n.a.	0.2	42	9.0
Batch 1h	2.5	250	12	0.70	2.0	1.9	1.3	0.17	0.53	0.48	n.a.	19	n.a.

n.a. = not applicable. Note: The reaction conditions of these experiments can be found in the captions of Fig. 2, 3, 4, 5, 6 and S11 at ESI.†

reported.[64–66] The N_2 sorption isotherms of the parent carbonized NDC and 35Ni/NDC represent type IV isotherms (Fig. S15 in the ESI†), which is characteristic of mesoporous materials. NDC and 35Ni/NDC exhibited high specific surface areas of 755 m^2 g^{-1} and 578 m^2 g^{-1} (Table S4 in the ESI†), respectively. This combined with a C/N ratio of 22 indicates relatively high N doping (Table S4 in the ESI†). XRD of the 35Ni/NDC catalyst showed the typical reflection of Ni^0 at 44° and 51°, indicating the complete reduction of NiO formed in the calcination step, *viz.* Fig. S16 in the ESI.† The HR-TEM images also showed Ni nanoparticles of the expected size, *i.e.* 20–40 nm, *viz.* Fig. S17 in the ESI.† These findings are in agreement with the crystalline size from CO-TPD of 21 nm, which is correlated to the Ni surface area of 21 m^2 g^{-1}, *cf.* Table S4 in the ESI.†

In this part, the influence of coupling a catalytic hydrogenolysis/hydrogenation step with the abovementioned solvothermal treatment on LS depolymerization was investigated. Herein, the presence of a redox catalyst (35Ni/NDC) facilitates LS depolymerization through hydrogenolysis of ether bonds of LS fragments, mostly β–O–4, and 4–O–5 (*viz.* Fig. S18 in the ESI†). Simultaneously, the unsaturated and unstable fragments formed solvothermally are catalytically hydrogenated, preventing their recondensation (*viz.* Fig. S18 in the ESI†).[59,81] For this purpose, a set of experiments was performed at three different reaction temperatures, *i.e.*, 150 °C, 200 °C and 250 °C, using water/alcohol with a weight ratio of 1 : 1, *i.e.*, EtOH/H_2O and MeOH/H_2O, as well as using only H_2O as a solvent. These experiments are noted as follows: SHF-MeOH/H_2O, SHF-EtOH/H_2O, and SHF-H_2O.

The dependence of the molecular weight (from SEC) on the reaction temperature in these experiments is shown in Fig. 4 and Fig. S19.† By increasing the reaction temperature from 150 °C to 200 °C and to 250 °C, the SEC elugrams showed a disappearance of the peak at low retention time (RT < 9 min), which corresponds to the high molecular weight fraction, in all solvent systems. Similarly, M_w and M_n exhibited significant decay when the temperature was increased from 150 °C to 200 °C and to 250 °C for SHF-MeOH/H_2O, SHF-MeOH/H_2O and SHF-H_2O, *viz.* Fig. 3, Fig. S19, and S20 in the ESI.† The M_w was found to have decreased from 12 390 g mol^{-1} (before reaction) to 433 g mol^{-1}, 502 g mol^{-1} and 1393 g mol^{-1} at 250 °C for SHF-MeOH/H_2O, SHF-EtOH/H_2O, and SHF-H_2O, respectively (Fig. 4 and Table S2 – entries 13 and 16 in the ESI†). All these values are smaller than those for SF (Table S2 – entries 4, 7 and 10 – in the ESI†).

Nevertheless, using pure H_2O as a solvent resulted in a higher molecular weight at all investigated temperatures compared to its water/alcohol counterparts. This observation is in agreement with the SF experiments, wherein using pure water as a solvent lead to the formation of oligomers and dimers.[77,82] Moreover, *Đ* has substantially decreased from 6.5 to 1.2 for SHF-MEOH/H_2O and SHF-EtOH/H_2O, and to 3.8 for SHF-H_2O *i.e.*, from highly dispersed to relatively monodisperse (Table S2 – entries 4 and 13 in the ESI†). This decrease of both *Đ* and M_w in SHF clearly indicates a controlled and efficient LS
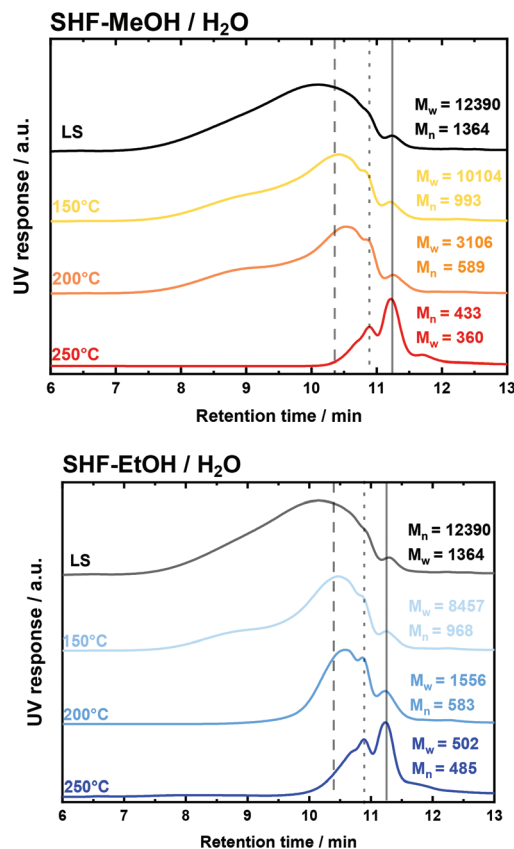

Fig. 4 SEC elugrams for SHF of LS using MeOH/H_2O (top) and EtOH/H_2O (bottom). Reaction conditions: c_{LS} = 1.0 wt%, T = 150 °C, 200 °C and 250° C, p = 7.0 MPa, Q_{educt} = 1.0 cm^3 min^{-1}, Q_{H_2} = 20 cm^3 min^{-1}, $m_{35Ni/NDC}$ = 10.0 g, $t_{residence}$ = 50 min, and weight hour space velocity (WHSV) = 0.17 g_{LS} h^{-1} g_{Ni}^{-1}. The straight line indicates the eluents buffer reference peak (NaHPO$_3$), dotted and dashed lines show the analytical standard peaks, *i.e.*, sodium polystyrene sulfonate, with M_w of 246 g mol^{-1} (RT = 10.9 min) and M_w of 891 g mol^{-1} (RT = 10.4 min), respectively.

depolymerization in the presence of the catalyst with respect to SF. These observations are in good agreement with the proposed stabilization of the formed monomers *via* hydrogenolysis/hydrogenation due to the presence of both H_2 and the redox catalyst. Thus, this step is required to prevent recondensation of the fragmented fraction.[59,81]
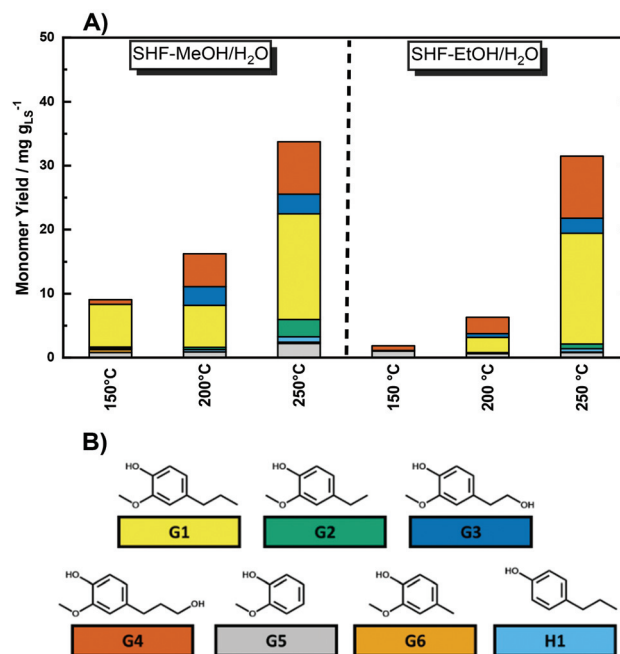
For detailed insights into the structure of the sample taken from SHF-MeOH/H_2O at 250 °C, characterization of the freeze dried solid residue (denoted as SHF-LS) was performed *via* elemental analysis (EA) including analysis of Na, Ca, and Mg *via* ICP-OES, FTIR and 2D HSQC NMR. The EA showed a decrease of the S content from 7.0 wt% to 5.0 wt%, while the O content decreased slightly from 36 wt% to 34 wt%, *cf.* Table 1. Differently, the Na, Ca and Mg amounts in the freeze-dried solid residue remained constant before and after the experiment. The difference in the S content is attributed to the elimination of sodium sulfate and sodium sulfide as a result of sulfonate hydrolysis and reduction. We also find a slightly higher acidity of the product solution (pH = 5.5) when com-

pared to the reactant solution (pH = 6.3). It is important to note that at this pH, the water soluble phenolates are not formed without subsequent loss of aromatics in the water phase. The 2D HSQC NMR spectra for SHF-LS showed the disappearance of the sulfo-group signals (α-$S_{\alpha,\beta,\gamma}$ at δ_C/δ_H 66–68/4.5–4.7, 79–82/4.7–5.1 and 60–62/3.9–4.0), which is an indication of the sulfonate group removal from LS (Fig. S21 in the ESI†). In addition, low intensity of Ni_2S_3 with respect to Ni^0 was found in the XRD pattern of the spent catalyst indicating a small amount of S^{2-} reacting on the catalyst surface (Fig. S22 in the ESI†), which however does not influence the catalyst performance, as proven by SEC and monomers yield. In addition, FTIR analysis of SHF samples showed a decrease of the O=S=O stretching bands at 1036 cm^{-1} and at around 1200 cm^{-1}, when compared to the original FTIR spectrum of LS, *viz.* Fig. S9 and Table S1 in the ESI.† Moreover, FTIR showed that the C–H stretching modes at 2954 and 2937 cm^{-1} exhibited a higher peak intensity in SHF samples than in the original LS. This suggests a higher concentration of alkyl chains in the SHF sample due to the LS hydrogenolysis/hydrogenation.

In order to evaluate the depolymerization efficiency at different temperatures, the SHF product has been qualitatively and quantitatively analyzed using GC-MS and GC-FID, respectively. By GC-MS it was possible to identify a wide range of monomers (18 compounds), as reported in Table S5 in the ESI.† Among the identified compounds, 4-propyl guaiacol (G1), 4-ethyl guaiacol (G2), homovanillyl alcohol (G3), dihydroconiferyl alcohol (G4), guaiacol (G5), creosol (G6), and 4-propyl phenol (H1) were the predominant ones and have been quantified from GC-FID chromatograms (Table 2, and Fig. S13 and S22 in the ESI†). Interestingly, the compounds with unsaturated alkene tails, *i.e.*, eugenol (G7) and isoeugenol (G8), *viz.* Fig. S14 in the ESI,† were found only in traces, indicating the efficient hydrogenation of the double bonds at the alkene tails using 35Ni/NDC. At a reaction temperature of 150 °C, the cumulative monomers yield (Y_{CM}) was found to be 9.1 mg g$_{LS}$$^{-1}$, 1.7 mg g$_{LS}$$^{-1}$ and 0.1 mg g$_{LS}$$^{-1}$ with MeOH/H$_2$O, EtOH/H$_2$O and H$_2$O as the solvent, respectively (Fig. 5, Table 2, and Fig. S24 and S25 in the ESI†). These compounds have boiling points between 200 °C and 300 °C, which allows them to be separated from the product mixture for further chemocatalytic upgrading.[28,83] Alternatively, separation based on solvent extraction can be performed.[28,63,83,84] Once separated, the monomer can be valorised toward phenols and alkenes *via* hydroprocessing and dealkylation, while the oligomers can be used for materials applications.[23,63]

Increasing the temperature from 150 °C to 200 °C and 250 °C corresponded to an increase in the Y_{CM} from 9.1 mg g$_{LS}$$^{-1}$ to 16 mg g$_{LS}$$^{-1}$ and to 34 mg g$_{LS}$$^{-1}$ for SHF-MeOH/H$_2$O mixtures and from 1.7 mg g$_{LS}$$^{-1}$ to 6.3 mg g$_{LS}$$^{-1}$ and to 31 mg g$_{LS}$$^{-1}$ for SHF-EtOH/H$_2$O, which correspond to the space–time cumulative monomer yield (STY$_{CM}$) of 1.6, 2.7, and 5.8 mg h^{-1} g$_{Ni}$$^{-1}$ for MeOH/H$_2$O and 0.29, 1.1, and 5.3 mg h^{-1} g$_{Ni}$$^{-1}$ for EtOH/H$_2$O. In contrast, SHF-H$_2$O exhibited a minimal Y_{CM} increase from 0.1 mg g$_{LS}$$^{-1}$ to 0.7 mg g$_{LS}$$^{-1}$ and to 1.7 mg g$_{LS}$$^{-1}$

Fig. 5 (A) Monomer yield for the SHF-MeOH/H$_2$O and SHF-EtOH/H$_2$O as a function of temperature; reaction conditions: c_{LS} = 1.0 wt%, T = 150 °C, 200 °C and 250° C, p = 7.0 MPa, Q_{educt} = 1.0 cm^3 min^{-1}, Q_{H_2} = 20 cm^3 min^{-1}, $m_{35Ni/NDC}$ = 10 g, $t_{residence}$ = 50 min, and weight hour space velocity (WHSV) = 0.17 g$_{LS}$ h^{-1} g$_{Ni}$$^{-1}$. (B) Structure of the quantified monomers.

at 150 °C, 200 °C, and 250 °C, respectively, *viz.* Fig. S25 in the ESI.† This lower Y_{CM} using pure H$_2$O instead of the water/alcohol mixture is in agreement with the previous study conducted with lignin[77,82] In this context, low Y_{CM} is attributed to the poor solubility of the formed monomers in water, which lead to their adsorption on the catalyst surface, which subsequently led to low Y_{CM} with respect to the water/alcohol solvent mixture.[82] Moreover, the hydrogenation of phenols in pure H$_2$O can lead to over-hydrogenation toward hexanols.[85] This is confirmed by the presence of only four monomers among the previously identified compounds, *i.e.* G2, G3 G5, and H, *viz.* Fig. S25 in the ESI.† The low Y_{CM} combined with the high M_w of the SHF-H$_2$O experiment indicates the necessity of using the water/alcohol mixture. In all the cases using alcohol/water mixtures, except EtOH/H$_2$O at 150 °C, the monomers were similarly distributed with 4-propyl guaiacol (G1) and dihydroconiferyl alcohol (G4) as the major products, *viz.* Fig. 5. However, the dominant distribution of phenolic monomers with reduced tail, such as G1–G6 and H1, indicates the effective hydrogenolysis/hydrogenation of LS fragments in the SHF process by the 35Ni/NDC catalyst. Nevertheless, it is important to underline that the selected compounds do not represent the entire amount of phenolic monomers, and for this reason, the cumulative monomer yield remains under-estimated. The values of monomer yield in both water/alcohol solvent systems at low temperature, *i.e.*, at 150 °C and 200 °C, are in-line with the maximum theoretical yield (~10 mg g$_{LS}$$^{-1}$)

that Rinaldi *et al.* reported only for the β–O–4 linkages of LS, indicating the cleavage of these linkage types.[30] However, at 250 °C, the cumulative monomer yield was found to be three times higher than the maximum theoretical yield, indicating the cleavage of other linkages in addition to β–O–4. These observations indicate that at 150 °C and 200 °C, depolymerization occurs mostly *via* hydrogenolysis of ether bonds. Whereas at 250 °C, in addition to β–O–4, a wide number of linkages, *e.g.*, 4–O–5 and 5–5 bonds, are cleaved solvothermally followed by the stabilization of the unsaturated bonds, *viz* in Fig. S26 in the ESI.† This process is within the typical lignin fragmentation at high temperatures (250–400 °C).[79,86] The solvothermal cleavage of bonds produces unstable intermediates, such as radicals and double bonds, which are hydrogenated using 35Ni/NDC, *viz.* Fig. S26 in the ESI.† This proposed scheme would confirm the protective action against recondensation of the 35Ni/NDC catalyst. For the catalytic hydrogenolysis of β–O–4 and 4–Ov5 ether bonds, we proposed that these steps are following a classical hydrogenation mechanism. This mechanism based on dissociative H_2 adsorption on Ni followed by LS adsorption and bond cleavage, is analogous to those of studies in the literature conducted with model compounds, *viz* Fig. S27.†[87–89]

In the studied system, the SHF-MeOH/H_2O solvent mixture showed a higher monomer yield over all temperature ranges than SHF-EtOH/H_2O. The higher activity of MeOH/H_2O confirms the results of the LS experiments and is attributed to the high polarity of this mixture that allows better solubility of LS, which led to high diffusion of LS through the 35Ni/NDC catalyst and higher LS hydrogenolysis/hydrogenation rates. These findings are in strong agreement with other studies conducted with MeOH on catalytic lignin depolymerization reported by the Sels group.[76,90] This demonstrated the crucial role of a polar solvent in lignin solubilization which could lead to improved process efficiency. Therefore, MeOH/H_2O has been selected for further investigations as the solvent mixture, due to its higher Y_{CM} when compared to EtOH/H_2O or pure H_2O.

Process optimization

In order to maximize the efficiency of LS depolymerization toward monomers, an experiment has been performed with a higher LS concentration (2.5 wt%) than in previous SF and SHF (1.0 wt%) experiments at 250 °C. It is important to mention that 2.5 wt% was chosen as the highest concentration, *i.e.*, it is the highest limit of LS solubility in the used solvent mixture (MeOH/H_2O) at room temperature.

In terms of weight hourly space velocity (WHSV), increasing the concentration from 1 to 2.5 wt% corresponded to an increase from 0.17 to 0.43 g_{LS} h^{-1} g_{Ni}^{-1}. Herein, M_w and M_n of 430 and 391 g mol^{-1} with $Đ$ of 1.1, respectively, were found (see Table 3). These values are comparable to the one obtained from the experiment conducted using 1.0 wt% LS solution (Table 3). Also, the cumulative monomer yield was found to be similar in both cases. These results show no significant influence of the higher concentration (from 1.0 wt% to 2.5 wt%) of LS on the catalyst performance. Accordingly, increasing the concentration from 1 to 2.5 wt% corresponded to an increase of STY_{CM} from 5.8 to 14 mg h^{-1} g_{Ni}^{-1}. Because of the higher weight productivity, the 2.5 wt% concentration was selected to investigate the catalyst stability over time on stream (TOS), *viz.* Fig. S28 in the ESI.† Exposing the 35Ni/NDC catalyst to the reaction conditions for 9 h, did not affect the Y_{CM}, which was found to be constant (*ca.* 30 mg g_{LS}^{-1}). However, the N_2 physisorption of 35Ni/NDC-TOS exhibited a loss in specific surface area from 578 to 272 m^2 g^{-1} (Fig. S29 in the ESI†). This decrease in the surface area indicates product deposition onto the catalysts, due to the affinity between aromatics and porous carbon, which is in agreement with a similar study conducted by our group for vanillin hydrogenation.[68] The XRD diffraction patterns of the spent catalyst after 9 h of TOS (35Ni/NDC-TOS) showed similar peaks to those of the spent catalyst after 1 h (Fig. S22 in the ESI†), with mainly Ni^0 reflections and the presence of $Ni(OH)_2$ and Ni_3S_2 phases. This remarkable resistance of Ni^0 for such a long time under harsh conditions (250 °C and the presence of S), is attributed to the establishment of a Mott–Schottky stabilization effect between the Ni^0 and the N of the carbon support.[68,91,92]
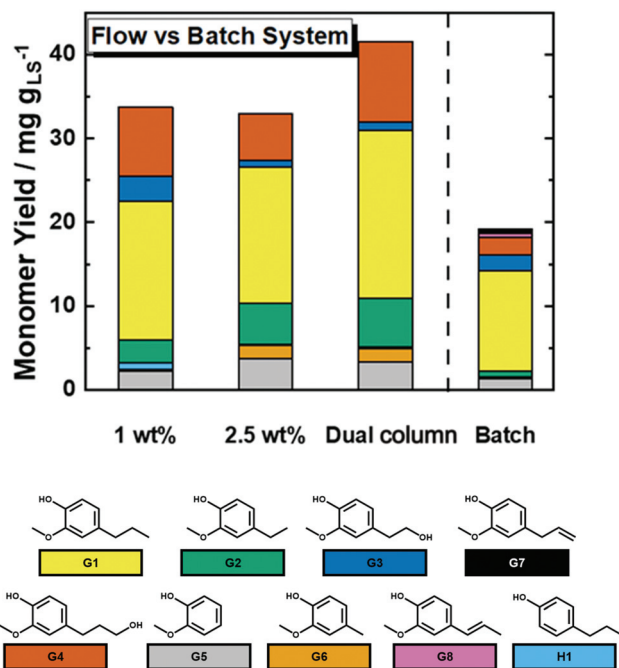
One of the advantages of operating in continuous flow systems is the possibility to couple multiple reactors together.[67] Herein, two identical packed reactors with 35Ni/NDC have been coupled in series, in order to prolong the contact time between the LS solution and the catalyst and consequently optimize the monomer yield (Fig. 6 and Fig. S5 in the ESI†). Moreover, coupling two flow reactors in series aims to mimic an industrial scale up of such process. Therein, the concentrated 2.5 wt% LS solution has been continuously fed through two coupled reactors packed with 35Ni/NDC. Accordingly, the double amount of the catalyst is used, result-

Table 3 SHF experiments using the MeOH/H_2O solvent mixture

Sample	M_w^a/g mol^{-1}	M_n^a/g mol^{-1}	$Đ^a$/—	Y_{CM}^b/mg g_{LS}^{-1}	STY_{CM}^b/mg $h^{-1}g_{Ni}^{-1}$
LS	12 390	1364	9.1	n.a.	n.a
SHF-MeOH/H_2O	433	360	1.2	34	5.8
Flow 2.5 wt%	430	391	1.1	33	14
Dual column	393	337	1.1	42	9.0
Batch 1 h	1615	491	3.3	19	n.a.
Batch 3 h	6942	684	10	n.d.^{c}	n.a

n.a. = not applicable. ^{a} Calculated by SEC. ^{b} Calculated from GC-FID results. ^{c} Not determined as the M_w is high with respect to 1 h.

Fig. 6 Monomers yield derived from the SHF-MeOH/H$_2$O in the continuous flow system with one and dual reactors and in a batch reactor. Continuous flow system with one tubular reactor; reaction conditions: c_{LS} = 1.0 and 2.5 wt%, T = 250° C, p = 7.0 MPa, Q_{educt} = 1.0 cm^3 min^{-1}, Q_{H_2} = 20 cm^3 min^{-1}, $m_{35Ni/NDC}$ = 10 g, $t_{residence}$ = 50 min, and weight hour space velocity (WHSV) = 0.17 and 0.43 g$_{LS}$ h^{-1} g$_{Ni}$$^{-1}$. Dual column continuous flow system; reaction conditions: c_{LS} = 2.5 wt%, T_1 and T_2 = 250° C, p_{system} = 7.0 MPa, Q_{educt} = 1.0 cm^3 min^{-1}, Q_{H_2} = 20 cm^3 min^{-1}, $m_{35Ni/NDC}$ in R_1 and R_2 = 10 g, $t_{residence}$ = 100 min, and weight hour space velocity (WHSV) = 0.21 g$_{LS}$ h^{-1} g$_{Ni}$$^{-1}$. Batch system; reaction conditions: c_{LS} = 2.5 wt%, V_{educt} = 30 cm^3, T = 250° C, p_{H_2} = 7.0 MPa, n = 400 rpm, $m_{35Ni/NDC}$ = 1 g and $t_{reaction}$ = 60 min.

ing in two-times lower WHSV (from 0.43 to 0.21 g$_{LS}$ h^{-1} g$_{Ni}$$^{-1}$). The molecular weight distributions in this experiment showed a slight decrease when compared with the sole reactor experiment using 2.5 wt% (Table 3). In contrast, the cumulative monomer yield increased from 33 to 42 mg g$_{LS}$$^{-1}$ when compared to the single column experiment (Fig. 6 and Table 2), *i.e.* prolonging the residence time resulted in an improved monomer yield. In addition, this monomer yield (42 mg g$_{LS}$$^{-1}$) is four times higher than the maximum theoretical monomer yield (~10 mg g$_{LS}$$^{-1}$) reported by Rinaldi *et al.* based on the cleavage of β–O–4 linkages in LS.[30] However, the benefits of using two columns in terms of Y_{CM} are combined with STY decreasing from 14 to 9.0 mg h^{-1} g$_{Ni}$$^{-1}$, *viz.* Table 3. This indicates that an excess amount of the catalyst is used in the dual columns experiment, with a non-optimized WHSV.

Comparison between batch and flow

To identify the assumed advantages of continuous flow over batch systems, catalytic LS depolymerization was performed in a batch system using the MeOH/H$_2$O solvent system. 1 h reaction time has been set to be comparable to the one in the flow system, yielding a M_w of 1615 g mol^{-1} and a Đ of 3.3 (Table 3).

These values are considerably higher than the ones in the flow system experiment. In addition, the cumulative monomer yield was found to be 19 mg g$_{LS}$$^{-1}$, which is lower than that for the continuous flow system (33 mg g$_{LS}$$^{-1}$ using 2.5 wt% LS solution), *viz.* Fig. 6 and Table 2. Interestingly, the batch systems showed the presence of monomer with an unsaturated alkene tail, *i.e.*, eugenol and isoeugenol, which could be a sign of the beginning of catalyst deactivation. Moreover, increasing the reaction time from 1 h to 3 h, corresponded to an increase of M_w from 1615 g mol^{-1} to 6942 g mol^{-1} as a result of catalyst deactivation, combined with an increase of Đ from 3.3 to 10. These findings are attributed to the fragment re-polymerization in a batch system that also leads to catalyst deactivation due to longer contact times between reactants and products.[93]

Conclusions

Industrial sodium lignosulfonate (LS) was successfully valorized using solvothermal fragmentation independently and combined with catalytic hydrogenolysis/hydrogenation in continuous flow systems. The depolymerization was found to occur thermally in the absence of the catalyst, rather independent of the solvent mixture. The decrease of molecular weight has been found to depend on the reaction temperature, *i.e.*, LS at those temperatures is an unstable polymer and shows ceiling behaviour. This allows direct and simple tuning of molecular weights of the formed fractions based on reaction temperatures. To obtain monomers and lower molecular weight fractions, the solvothermal fragmentation should be coupled with a catalytic hydrogenolysis/hydrogenation step. An optimum cumulative monomer yield of 34 mg g$_{LS}$$^{-1}$ (STY of 5.8 mg h^{-1} g$_{Ni}$$^{-1}$) has been found at 250 °C using MeOH/H$_2$O as a solvent, while indeed most of the fragments are in the dimer and trimer range, which is more exciting from a polymer perspective. Moreover, the presence of a hydrogenation catalyst allowed a higher degree of depolymerization even at a lower temperature. This clearly showed that 35Ni/NDC plays a vital role in this approach, as it is responsible for further fragmentation through hydrogenolysis/hydrogenation steps.

Extending the residence time by coupling two reactors yielded an even higher cumulative monomer yield of 42 mg g$_{LS}$$^{-1}$ with respect to the experiment in a single tubular reactor. However, the decreased STY of this approach (9.0 mg h^{-1} g$_{Ni}$$^{-1}$) pointed out the need for higher weight productivity in view of further possible improvements.

The obtained monomer yield is relatively low, but also expected and well-known for technical lignin.[30] This is due to the high sulfonate (and counter-ion) content, as well as the low amount of C–O bonds of LS when compared to native lignin.[30] This is the intrinsic limitation of using technical lignin as the starting feedstock for lignin depolymerization. Nevertheless, in our contribution, we reported on a high cumulative monomer yield when it is compared to other work presented in the literature using similar lignin.[52,53]

In addition to the monomers, the SHF process simultaneously produces lignin oligomers, which can be also applied in a wide range of applications. Based on this, we believe that our approach has the potential to use both the monomer and the oligomers fractions, moreover the weight of the product solutions can be tuned according to the temperature.

We also have to underline that all these data were obtained using an industrial LS waste, *i.e.*, containing 7.0 wt% sulfur and 10 wt% sodium, rather than impurity-free lignin. Certainly, other lignin types could allow high targeted monomer yields. Nevertheless, giving value to industrial waste will increase the sustainability of already established biorefinery processes and accelerate the transition toward a sustainable circular bio-economy.

Conflicts of interest

The authors declare that they have no known competing financial interests or personal relationships that could have appeared to influence the work reported in this paper.

Acknowledgements

References

1 A. Katelhon, R. Meys, S. Deutz, S. Suh and A. Bardow, *Proc. Natl. Acad. Sci. U. S. A.*, 2019, **116**, 11187–11194.

2 M. Al-Naji, J. Van Aelst, Y. Liao, M. d'Hullian, Z. Tian, C. Wang, R. Gläser and B. F. Sels, *Green Chem.*, 2020, **22**, 1171–1181.

3 M. Al-Naji, A. Yepez, A. M. Balu, A. A. Romero, Z. Chen, N. Wilde, H. Li, K. Shih, R. Gläser and R. Luque, *J. Mol. Catal. A: Chem.*, 2016, **417**, 145–152.

4 M. Al-Naji, M. Popova, Z. Chen, N. Wilde and R. Gläser, *ACS Sustainable Chem. Eng.*, 2019, **8**, 393–402.

5 C. O. Tuck, E. Pérez, I. T. Horváth, R. A. Sheldon and M. Poliakoff, *Science*, 2012, **337**, 695–699.

6 R. A. Sheldon, *ACS Sustainable Chem. Eng.*, 2017, **6**, 32–48.

7 S. Pacala and R. Socolow, *Science*, 2004, **305**, 968–972.

8 B. Kumru, J. A. Mendoza Mesa, M. Antonietti and M. Al-Naji, *ACS Sustainable Chem. Eng.*, 2019, **7**, 17574–17579.

9 M. Al-Naji, H. Schlaad and M. Antonietti, *Macromol. Rapid Commun.*, 2020, 2000485, DOI: 10.1002/marc.202000485.

10 J. A. Mendoza Mesa, F. Brandi, I. Shekova, M. Antonietti and M. Al-Naji, *Green Chem.*, 2020, **22**, 7398–7405.

11 P. Anastas and N. Eghbali, *Chem. Soc. Rev.*, 2010, **39**, 301–312.

12 M. M. Abu-Omar, K. Barta, G. T. Beckham, J. Luterbacher, J. Ralph, R. Rinaldi, Y. Roman-Leshkov, J. Samec, B. Sels and F. Wang, *Energy Environ. Sci.*, 2021, **14**, 262–292.

13 A. Corma, S. Iborra and A. Velty, *Chem. Rev.*, 2007, **107**, 2411–2502.

14 M. Besson, P. Gallezot and C. Pinel, *Chem. Rev.*, 2014, **114**, 1827–1870.

15 F. H. Isikgor and C. R. Becer, *Polym. Chem.*, 2015, **6**, 4497–4559.

16 D. Esposito and M. Antonietti, *Chem. Soc. Rev.*, 2015, **44**, 5821–5835.

17 J. Martin and M. Haggith, Enviromental Paper Network: The State of Global Paper Industry https://www.environmentalpaper.org, (accessed 27 January 2021).

18 C. E. Wyman, B. E. Dale, R. T. Elander, M. Holtzapple, M. R. Ladisch and Y. Lee, *Bioresour. Technol.*, 2005, **96**, 1959–1966.

19 A. J. Ragauskas, G. T. Beckham, M. J. Biddy, R. Chandra, F. Chen, M. F. Davis, B. H. Davison, R. A. Dixon, P. Gilna, M. Keller, P. Langan, A. K. Naskar, J. N. Saddler, T. J. Tschaplinski, G. A. Tuskan and C. E. Wyman, *Science*, 2014, **344**, 1246843–1246843.

20 H. Sadeghifar and A. Ragauskas, *ACS Sustainable Chem. Eng.*, 2020, **8**, 8086–8101.

21 T. Aro and P. Fatehi, *ChemSusChem*, 2017, **10**, 1861–1877.

22 P. C. A. Bruijnincx, R. Rinaldi and B. M. Weckhuysen, *Green Chem.*, 2015, **17**, 4860–4861.

23 Y. Liao, S.-F. Koelewijn, G. Van den Bossche, J. Van Aelst, S. Van den Bosch, T. Renders, K. Navare, T. Nicolaï, K. Van Aelst, M. Maesen and B. Sels, *Science*, 2020, **367**, 1385–1390.

24 E. Paone, T. Tabanelli and F. Mauriello, *Curr. Opin. Green Sustainable Chem.*, 2020, **24**, 1–6.

25 S. S. Hassan, G. A. Williams and A. K. Jaiswal, *Renewable Sustainable Energy Rev.*, 2019, **101**, 590–599.

26 P. C. Bruijnincx, R. Rinaldi and B. M. Weckhuysen, *Green Chem.*, 2015, **17**, 4860–4861.

27 Z. Sun, B. Fridrich, A. de Santi, S. Elangovan and K. Barta, *Chem. Rev.*, 2018, **118**, 614–678.

28 W. Schutyser, T. Renders, S. Van den Bosch, S. F. Koelewijn, G. T. Beckham and B. F. Sels, *Chem. Soc. Rev.*, 2018, **47**, 852–908.

29 J. E. Holladay, J. F. White, J. J. Bozell and D. Johnson, *Top value-added chemicals from biomass-Volume II—Results of*

screening for potential candidates from biorefinery lignin, Pacific Northwest National Lab.(PNNL), Richland, WA (United States), 2007.

30 R. Rinaldi, R. Jastrzebski, M. T. Clough, J. Ralph, M. Kennema, P. C. A. Bruijnincx and B. M. Weckhuysen, *Angew. Chem., Int. Ed.*, 2016, **55**, 8164–8215.

31 J. Zakzeski, P. C. Bruijnincx, A. L. Jongerius and B. M. Weckhuysen, *Chem. Rev.*, 2010, **110**, 3552–3599.

32 H. Kobayashi, H. Ohta and A. Fukuoka, in *Catalytic Hydrogenation for Biomass Valorization*, ed. R. Rinaldi, RCS Energy and Environment Series No. 13, 2015, pp. 52–71.

33 A. Llevot, P. K. Dannecker, M. von Czapiewski, L. C. Over, Z. Soyler and M. A. Meier, *Chem. – Eur. J.*, 2016, **22**, 11510–11521.

34 A. Llevot, E. Grau, S. Carlotti, S. Grelier and H. Cramail, *Macromol. Rapid. Commun.*, 2016, **37**, 9–28.

35 Z. Strassberger, S. Tanase and G. Rothenberg, *RSC Adv.*, 2014, **4**, 25310–25318.

36 S. Laurichesse and L. Avérous, *Prog. Polym. Sci.*, 2014, **39**, 1266–1290.

37 Z. Sun, J. Cheng, D. Wang, T. Q. Yuan, G. Song and K. Barta, *ChemSusChem*, 2020, **13**(19), 5199–5212.

38 I. F. Demuner, J. L. Colodette, A. J. Demuner and C. M. Jardim, *Bioresour. Technol.*, 2019, **14**(3), 7543–7581.

39 J. Ruwoldt, *Surfaces*, 2020, **3**, 622–648.

40 P. Fatehi and Y. Ni, in *Sustainable Production of Fuels, Chemicals, and Fibers from Forest Biomass*, ed. B. Zhu, ACS Symposium Series; American Chemical Society, Washington, DC, 2011.

41 M. Y. A. Mollah, W. Yu, R. Schennach and D. L. Cocke, *Cem. Concr. Res.*, 2000, 267–273, DOI: 10.1016/S0008-8846(99)00243-4.

42 L. Hu, Y. Zhou, M. Zhang and R. Liu, *BioResources*, 2012, **7**, 554–564.

43 Borregaard, Potential applications for different lignin sources based on experience from Borregaard, https://www.google.com/url?sa=t&rct=j&q=&esrc=s&source=web&cd=&ved=2ahUKEwit0eSf7KruAhURahQKHRtFCFoQFjAAegQIBxAC&url=http%3A%2F%2Fwww.lth.se%2Ffileadmin%2Fenergiportalen%2FEnergy_Portal%2FFiles%2FPres_Rodsrud.pdf&usg=AOvVaw2jH3uyvQBINJ-PiQySZp9l, (accessed 27 January 2021).

44 Y. Qin, D. Yang and X. Qiu, *ACS Sustainable Chem. Eng.*, 2015, **3**, 3239–3244.

45 S. Gao, Z. Cheng, X. Zhou, Y. Liu, R. Chen, J. Wang, C. Wang, F. Chu, F. Xu and D. Zhang, *Int. J. Biol. Macromol.*, 2020, **161**, 755–762.

46 B. V. K. J. Schmidt, V. Molinari, D. Esposito, K. Tauer and M. Antonietti, *Polymer*, 2017, **112**, 418–426.

47 C. Che, M. Vagin, U. Ail, V. Gueskine, J. Phopase, R. Brooke, R. Gabrielsson, M. P. Jonsson, W. C. Mak, M. Berggren and X. Crispin, *Adv. Sustainable Syst.*, 2019, **3**, 1900039.

48 R. Guterman, V. Molinari and E. Josef, *Angew. Chem., Int. Ed.*, 2019, **58**, 13044–13050.

49 X. Zhang, A. L. Licon, T. I. Harris, P. F. Oliveira, B. J. McFarland, B. E. Taurone, B. J. Walsh, B. E. Bell, C. T. Walker, R. V. Lewis and J. A. Jones, *ACS Omega*, 2019, **4**, 4832–4838.

50 J. Pang, W. Zhang, H. Zhang, J. Zhang, H. Zhang, G. Cao, M. Han and Y. Yang, *Carbon*, 2018, **132**, 280–293.

51 V. Molinari and M. Antonietti, Lignin-based composite materials and methods for its preparation, *European patent office Patent No* EP 3 266 810 A1, 2018.

52 J. Horáček, J.-P. Mikkola, A. Samikannu, G. Šťávová, W. Larsson, L. Hora and D. Kubička, *Top. Catal.*, 2013, **56**, 794–799.

53 R. Shu, Y. Xu, L. Ma, Q. Zhang, T. Wang, P. Chen and Q. Wu, *RSC Adv.*, 2016, **6**, 88788–88796.

54 Q. Song, F. Wang and J. Xu, *Chem. Commun.*, 2012, **48**, 7019–7021.

55 P. Cui, H.-X. Fang, C. Qian and M.-H. Cheng, *Chromatographia*, 2019, **83**, 87–93.

56 M. Fache, B. Boutevin and S. Caillol, *ACS Sustainable Chem. Eng.*, 2015, **4**, 35–46.

57 K. Van Aelst, E. Van Sinay, T. Vangeel, E. Cooreman, G. Van den Bossche, T. Renders, J. Van Aelst, S. Van den Bosch and B. F. Sels, *Chem. Sci.*, 2020, **11**, 11498–11508.

58 S. Van den Bosch, S. F. Koelewijn, T. Renders, G. Van den Bossche, T. Vangeel, W. Schutyser and B. Sels, in *Lignin Chemistry*, ed. L. Serrano, R. Luque and B. Sels, Springer Nature Switzerland, Cham, 2020, pp. 129–168.

59 T. Renders, G. Van den Bossche, T. Vangeel, K. Van Aelst and B. Sels, *Curr. Opin. Biotechnol*, 2019, **56**, 193–201.

60 S. Van den Bosch, S. F. Koelewijn, T. Renders, G. Van den Bossche, T. Vangeel, W. Schutyser and B. F. Sels, in *Topics Curr Chem*, 2018, vol. 376.

61 T. Renders, S. Van den Bosch, S. F. Koelewijn, W. Schutyser and B. F. Sels, *Energy Environ. Sci.*, 2017, **10**, 1551–1557.

62 E. Cooreman, T. Vangeel, K. Van Aelst, J. Van Aelst, J. Lauwaert, J. W. Thybaut, S. Van den Bosch and B. F. Sels, *Ind. Eng. Chem. Res.*, 2020, **59**, 17035–17045.

63 Y. Liao, S. Van den Bosch, J. Van Aelst and B. Sels, Catalytic funneling of phenolics, *US Patent No* 17083154, 2021.

64 S. G. Parto, J. M. Christensen, L. S. Pedersen, A. B. Hansen, F. Tjosås, C. Spiga, C. D. Damsgaard, D. B. Larsen, J. Ø. Duus and A. D. Jensen, *Energy Fuels*, 2019, **33**, 1196–1209.

65 S. Ghafarnejad Parto, J. Munkholt Christensen, L. Saaby Pedersen, F. Tjosås and A. D. Jensen, *Catalysts*, 2018, **8**, 502.

66 M. L. Stone, E. M. Anderson, K. M. Meek, M. Reed, R. Katahira, F. Chen, R. A. Dixon, G. T. Beckham and Y. Román-Leshkov, *ACS Sustainable Chem. Eng.*, 2018, **6**, 11211–11218.

67 F. Brandi, I. Khalil, M. Antonietti and M. Al-Naji, *ACS Sustainable Chem. Eng.*, 2021, **9**, 927–935.

68 F. Brandi, M. Bäumel, V. Molinari, I. Shekova, I. Lauermann, T. Heil, M. Antonietti and M. Al-Naji, *Green Chem.*, 2020, **22**, 2755–2766.

69 F. Brandi, M. Bäumel, I. Shekova, V. Molinari and M. Al-Naji, *Sustainable Chem.*, 2020, **1**, 106–115.

70 M. Al-Naji, B. Puertolas, B. Kumru, D. Cruz, M. Baumel, B. Schmidt, N. V. Tarakina and J. Perez-Ramirez, *ChemSusChem*, 2019, **12**(12), 2628–2636.

71 O. Musl, I. Sulaeva, M. Bacher, A. K. Mahler, T. Rosenau and A. Potthast, *ChemSusChem*, 2020, **13**, 4595–4604.

72 B. F. Lutnaes, B. O. Myrvold, R. A. Lauten and M. M. Endeshaw, *Magn. Reson. Chem.*, 2008, **46**, 299–305.

73 M. Alonso, M. Oliet, F. Rodriguez, G. Astarloa and J. Echeverría, *J. Appl. Polym. Sci.*, 2004, **94**, 643–650.

74 K. Fukuhara, K. Nakajima, M. Kitano, S. Hayashi and M. Hara, *Phys. Chem. Chem. Phys.*, 2013, **15**, 9343–9350.

75 E. M. Anderson, M. L. Stone, R. Katahira, M. Reed, G. T. Beckham and Y. Román-Leshkov, *Joule*, 2017, **1**, 613–622.

76 W. Schutyser, S. Van den Bosch, T. Renders, T. De Boe, S. F. Koelewijn, A. Dewaele, T. Ennaert, O. Verkinderen, B. Goderis, C. M. Courtin and B. F. Sels, *Green Chem.*, 2015, **17**, 5035–5045.

77 T. Renders, S. Van den Bosch, T. Vangeel, T. Ennaert, S.-F. Koelewijn, G. Van den Bossche, C. M. Courtin, W. Schutyser and B. F. Sels, *ACS Sustainable Chem. Eng.*, 2016, **4**, 6894–6904.

78 X. Wang and R. Rinaldi, *ChemSusChem*, 2012, **5**, 1455–1466.

79 T. Watanabe, H. Kawamoto and S. Saka, *Holzforschung*, 2009, **63**, 424–430.

80 B. D. Mar, H. W. Qi, F. Liu and H. J. Kulik, *J. Phys. Chem. A*, 2015, **119**, 6551–6562.

81 Y. M. Questell-Santiago, M. V. Galkin, K. Barta and J. S. Luterbacher, *Nat. Rev. Chem.*, 2020, **4**, 311–330.

82 T. Renders, E. Cooreman, S. Van den Bosch, W. Schutyser, S. F. Koelewijn, T. Vangeel, A. Deneyer, G. Van den Bossche, C. M. Courtin and B. F. Sels, *Green Chem.*, 2018, **20**, 4607–4619.

83 O. D. Mante, D. C. Dayton and M. Soukri, *RSC Adv.*, 2016, **6**, 94247–94255.

84 J. S. Kim, *Bioresour. Technol.*, 2015, **178**, 90–98.

85 J. He, C. Zhao and J. A. Lercher, *J. Catal.*, 2014, **309**, 362–375.

86 X. Zhou, L. J. Broadbelt and R. Vinu, in *Thermochemical Process Engineering*, 2016, pp. 95–198, DOI: 10.1016/bs.ache.2016.09.002.

87 Y. Li, S. D. Karlen, B. Demir, H. Kim, J. Luterbacher, J. A. Dumesic, S. S. Stahl and J. Ralph, *ChemSusChem*, 2020, **13**, 4487–4494.

88 J. He, C. Zhao, D. Mei and J. A. Lercher, *J. Catal.*, 2014, **309**, 280–290.

89 J. He, C. Zhao and J. A. Lercher, *J. Am. Chem. Soc.*, 2012, **134**, 20768–20775.

90 J. H. Li, C. F. Lin, W. Qin, X. B. Xiao and L. Wei, *Acta Phys. – Chim. Sin.*, 2016, **32**, 2717–2723.

91 Z. H. Xue, J. T. Han, W. J. Feng, Q. Y. Yu, X. H. Li, M. Antonietti and J. S. Chen, *Angew. Chem., Int. Ed.*, 2018, **57**, 2697–2701.

92 X. H. Li and M. Antonietti, *Chem. Soc. Rev.*, 2013, **42**, 6593–6604.

93 S. M. G. Lama, J. Pampel, T.-P. Fellinger, V. P. Beškoski, L. Slavković-Beškoski, M. Antonietti and V. Molinari, *ACS Sustainable Chem. Eng.*, 2017, **5**, 2415–2420.